Neuroscience 279 (2014) 155–167

DISRUPTED TOPOLOGICAL PROPERTIES OF BRAIN WHITE MATTER NETWORKS IN LEFT TEMPORAL LOBE EPILEPSY: A DIFFUSION TENSOR IMAGING STUDY

Y. XU,[a†] S. QIU,[b†] J. WANG,[a] Z. LIU,[b] R. ZHANG,[a] S. LI,[a] L. CHENG,[c] Z. LIU,[d] W. WANG[c*] AND R. HUANG[a*]

[a] *Center for the Study of Applied Psychology, Key Laboratory of Mental Health and Cognitive Science of Guangdong Province, School of Psychology, South China Normal University, Guangzhou 510631, PR China*

[b] *Department of Medical Image Center, Nanfang Hospital, Southern Medical University, Guangzhou 510515, PR China*

[c] *Department of Medical Image Center, Guangdong 999 Brain Hospital, Guangzhou 510510, PR China*

[d] *School of Biomedical Engineering, Southern Medical University, Guangzhou 510515, PR China*

Abstract—Mesial temporal lobe epilepsy (mTLE) is the most common drug-refractory focal epilepsy in adults. Although previous functional and morphological studies have revealed abnormalities in the brain networks of mTLE, the topological organization of the brain white matter (WM) networks in mTLE patients is still ambiguous. In this study, we constructed brain WM networks for 14 left mTLE patients and 22 age- and gender-matched normal controls using diffusion tensor tractography and estimated the alterations of network properties in the mTLE brain networks using graph theoretical analysis. We found that networks for both the mTLE patients and the controls exhibited prominent small-world properties, suggesting a balanced topology of integration and segregation. However, the brain WM networks of mTLE patients showed a significant increased characteristic path length but significant decreased global efficiency, which indicate a disruption in the organization of the brain WM networks in mTLE patients. Moreover, we found significant between-group differences in the nodal properties in several brain regions, such as the left superior temporal gyrus, left hippocampus, the right occipital and right temporal cortices. The robustness analysis showed that the results were likely to be consistent for the networks constructed with different definitions of node and edge weight. Taken together, our findings may suggest an adverse effect of epileptic seizures on the organization of large-scale brain WM networks in mTLE patients.

key words: diffusion tensor imaging, temporal lobe epilepsy, graph theory, connectivity.

INTRODUCTION

Mesial temporal lobe epilepsy (mTLE) is the most common form of human medically intractable epilepsy, characterized by the epileptogenic focus and neuropathological changes in the mesial temporal regions (Engel, 2001). Most mTLE cases are associated with mesial temporal sclerosis (MTS), the usually pathologic substrate of which is hippocampal sclerosis (HS). Abundant neuroimaging studies have found that brain structural abnormalities can spread through neural networks to other regions such as the frontocentral, occipital, and parietal areas (Bernhardt et al., 2008, 2009, 2010; Keller and Roberts, 2008). Functional magnetic resonance imaging (MRI) studies also found abnormal activations in widespread regions in the temporal, parietal and occipital cortices in TLE (Waites et al., 2006; Voets et al., 2009; Alessio et al., 2013).

Advances in the development and application of diffusion tensor imaging (DTI) have allowed for investigating the organization of human brain white matter (WM) (Hagmann et al., 2008; Iturria-Medina et al., 2008; Gong et al., 2009a). Numerous DTI studies of TLE have reported brain WM abnormalities in TLE according to DTI analysis, such as the external capsule, corpus callosum (Meng et al., 2010), fornix, cingulum (Concha et al., 2009), uncinate fasciculus, arcuate fasciculus (Lin et al., 2008), and inferior fronto-occipital fasciculus (McDonald et al., 2008a).

Even though the widespread WM damage in TLE suggests disrupted structural integrity derived from a systemic disorder, few studies have investigated the disrupted WM organizations in TLE patients from a system level. Graph theoretical analysis offers a formal framework that can be used to quantify topological and organizational brain properties of complex networks (Bullmore and Sporns, 2009; Guye et al., 2010). Different topological parameters can be used to describe different aspects of the brain networks, such as the global

*Corresponding authors. Tel/fax: +86-20-8763-3769 (W. Wang). Tel/fax: +86-20-8521-6499 (R. Huang).
E-mail addresses: wangwensheng36@163.com (W. Wang), ruiwang.huang@gmail.com (R. Huang).

† These authors contributed equally to this work.

Abbreviations: AAL, automated anatomical labeling; DTI, diffusion tensor imaging; EEG, electroencephalogram; FA, fractional anisotropy; FDR, false discovery rate; FOV, field of view; HIP.L, left hippocampus; HS, hippocampal sclerosis; MNI, Montreal Neurological Institute; MD, mean diffusivity; MTG.R, right middle temporal gyrus; mTLE, mesial temporal lobe epilepsy; MRI, magnetic resonance imaging; MTS, mesial temporal sclerosis; SNR, signal-to-noise ratio; STG.L, left superior temporal gyrus; TE, echo time; TR, repetition time; TPOmid.R, middle temporal pole; WM, white matter.

http://dx.doi.org/10.1016/j.neuroscience.2014.08.040

Table 1. Cortical and subcortical regions of interest defined in this study using the automated anatomical labeling (AAL) atlas. These brain regions were originally described by Tzourio-Mazoyer et al. (2002). Abbreviations are listed according to Salvador et al. (2005) and Achard and Bullmore, 2007. Each of the left and right hemispheres contains 45 regions, respectively

Index	Regions	Abbr.	Index	Regions	Abbr.
1	Precentral gyrus	PreCG	24	Lingual gyrus	LING
2	Superior frontal gyrus, dorsolateral	SFGdor	25	Superior occipital gyrus	SOG
3	Superior frontal gyrus, orbital part	ORBsup	26	Middle occipital gyrus	MOG
4	Middle frontal gyrus	MFG	27	Inferior occipital gyrus	IOG
5	Middle frontal gyrus, orbital part	ORBmid	28	Fusiform gyrus	FFG
6	Inferior frontal gyrus, opercular part	IFGoperc	29	Postcentral gyrus	PoCG
7	Inferior frontal gyrus, triangular part	IFGtriang	30	Superior parietal gyrus	SPG
8	Inferior frontal gyrus, orbital part	ORBinf	31	Inferior parietal, but supra- marginal and angular gyri	IPL
9	Rolandic operculum	ROL	32	Supramarginal gyrus	SMG
10	Supplementary motor area	SMA	33	Angular gyrus	ANG
11	Olfactory cortex	OLF	34	Precuneus	PCUN
12	Superior frontal gyrus, medial	SFGmed	35	Paracentral lobule	PCL
13	Superior frontal gyrus, medial orbital	ORBsupmed	36	Caudate nucleus	CAU
14	Gyrus rectus	REC	37	Lenticular nucleus, putamen	PUT
15	Insula	INS	38	Lenticular nucleus, pallidum	PAL
16	Anterior cingulate and paracingulate gyri	ACG	39	Thalamus	THA
17	Median cingulate and paracingulate gyri	DCG	40	Heschl gyrus	HES
18	Posterior cingulate gyrus	PCG	41	Superior temporal gyrus	STG
19	Hippocampus	HIP	42	Temporal pole: superior temporal gyrus	TPOsup
20	Parahippocampal gyrus	PHG	43	Middle temporal gyrus	MTG
21	Amygdala	AMYG	44	Temporal pole: middle temporal gyrus	TPOmid
22	Calcarine fissure and surrounding cortex	CAL	45	Inferior temporal gyrus	ITG
23	Cuneus	CUN			

efficiency describing the brain functional integration and the local efficiency indicating the functional segregation among the nodes of brain networks (for detailed information of network measures, see Table 2). Recently, graph theoretical analyses of brain WM networks have also been applied to diverse psychiatric and neurological diseases, such as Alzheimer's disease (Lo et al., 2010), schizophrenia (Zalesky et al., 2011), multiple sclerosis (Shu et al., 2011), mild cognitive impairment (Bai et al., 2012), and chronic epilepsy (Vaessen et al., 2012). As to the application of graph theory to mTLE patients, Liu et al. constructed brain WM networks based on 78 brain cortical regions and observed obvious small-world properties in the left mTLE patients (Liu et al., 2014). A graph-theoretical analysis of MRI-based cortical thickness correlations reported that networks in patients with left and right TLE were characterized by a small-world topology (Bernhardt et al., 2011). Using resting-state fMRI, Liao et al. also found small-world attributes in TLE patients with bilateral MTS (Liao et al., 2010).

Our aim was to study the large-scale brain WM networks in mTLE patients using graph theoretical analysis. Following up on previous studies suggesting extensive brain network alterations in mTLE patients (Bernhardt et al., 2010; Alessio et al., 2013), we attempted to detect the disrupted topological organization and altered nodal properties in the whole-brain WM networks in mTLE patients.

EXPERIMENTAL PROCEDURES

Subjects

According to a comprehensive clinical evaluation including a careful interview, neurological examination, neuropsychological assessment, and neurophysiological monitoring, we recruited 22 TLE from the Guangdong 999 Brain Hospital. In order to avoid confounding factors from brain lesions, we set the exclusion criteria as: (1) MRI finding of intracranial space-occupying lesions (such as tumors, parasites, or vascular malformations), WM degeneration or other lesions; and (2) mismatch between the electroencephalogram (EEG) localization and the clinical evidence. Thus, we excluded eight patients and identified 14 patients as the left mTLE (four females; median age = 24 years old). All of these mTLE patients satisfied the following criteria: (1) MRI manifestation of left-sided HS; (2) standard EEG and video-EEG evaluations that clearly indicated interictal discharges in the left temporal lobe. We acquired both DTI and resting-state fMRI datasets from TLE patients in the same session. All patients had discontinued anti-epilepsy medication for about 24 h prior to the scans, and no seizure occurred during this period. Before the study, patients were on AED (anti-epileptic drugs) treatment, including levetiracetam, lamotrigine, topamax, carbamazepine, valproate, either in monotherapy or multitherapy.

We also recruited 22 healthy subjects (nine females; median age = 24.5 years) as the controls (age: *t*-test, $p = 0.74$; gender: χ^2-test, $p = 0.50$). None of them had any history of brain injury or cognitive problems. Both the left mTLE patients and the controls were right-handed and had normal or corrected-to-normal vision. Protocols of this study were approved by the Institutional Review Board of the Guangdong 999 Brain Hospital in Guangzhou. Written informed consent was obtained from all subjects prior to the MRI scanning.

Table 2. Formulae for the topological properties of a network. Their descriptions can be found in Rubinov and Sporns (2010)

	Parameters and formulae	Definitions
Small-world property	Normalized clustering coefficient $\gamma = C_p/C_p^{rand}$	C_p^{rand} is the mean weighted clustering coefficient of 100 matched random networks
	Normalized shortest path length $\lambda = L_p/L_p^{rand}$	L_p^{rand} is the mean weighted characteristic path length of 100 matched random networks
	Small-worldness $\sigma = \gamma/\lambda$	
Global parameters	Clustering coefficient $C_p = \frac{1}{N}\sum_i \frac{\sum_{j,k}(\overline{W}_{ij}\overline{W}_{jk}\overline{W}_{ki})^{1/3}}{K_i(K_i-1)}$	K_i is the degree of node i; $\overline{W}_{ij}$ is the weight scaled by the largest weight in the network, $\overline{W}_{ij} = W_{ij}/\max(W_{ij})$. N is the number of nodes in the network
	Characteristic path length $L_p = \frac{1}{N(N-1)}\sum_{i=1}^{N}\sum_{j\neq i}^{N} L_{ij}$	L_{ij} is defined as the length of the shortest path between node i and node j
	Global efficiency $E_{glob}(G) = \frac{1}{N(N-1)}\sum_{i=1}^{N}\sum_{j\neq i}^{N}\frac{1}{L_{ij}}$	L_{ij} is defined as the length of the shortest path between node i and node j
	Local efficiency $E_{loc}(G) = \frac{1}{N}\sum_{i\in G} E_{glob}(G_i)$	$E_{glob}(G_i)$ is the global efficiency of the neighborhood subgraph G_i of the node i
Nodal parameters	Nodal efficiency $E_{nodal}(i) = \frac{1}{N-1}\sum_{i\neq j\in G}\frac{1}{L_{ij}}$	L_{ij} is defined as the length of the shortest path between node i and node j
	Degree $K_i = \sum_{j\neq i\in G} w_{ij}$	W_{ij} is the edge weight between node i and node J
	Normalized betweenness centrality $B_i = b_i / < b_i >$	$< b_i >$ is the average nodal betweenness of the network. ρ_{jk} is the number of shortest paths between j and k, and $\rho_{jk}(i)$ is the number of shortest paths between j and k that pass through i
	Betweenness centrality $b_i = \frac{1}{(N-1)(N-2)}\sum_{i\neq j\neq k\in G}\frac{\rho_{jk}(i)}{\rho_{jk}}$	

Image acquisition

MRI data were acquired on a 1.5T Philips Intera MRI scanner. During the scanning, foam pads were used to reduce head motion. Diffusion-weighted images were obtained using a single-shot spin-echo EPI sequence with the following parameters: repetition time (TR) = 11,000 ms, echo time (TE) = 71.6 ms, slice thickness = 2 mm, field of view (FOV) = 230 mm × 230 mm and matrix size = 14 4 × 144, giving a voxel size of 1.6 × 1.6 × 2 mm^3, 31 non-collinear gradient directions with a b-value of 800 s/mm^2 and one additional volume without diffusion weighting (b = 0 s/mm^2), and 67 transverse slices without gap covering the whole brain. The scanning time for acquiring the DTI data was about 6 min. We also acquired 3D high-resolution brain structural images using a T1-weighted MP-RAGE sequence: TR = 25 ms, TE = 4.6 ms, slice thickness = 1.2 mm. FOV = 240 mm × 240 mm and matrix size = 256 × 256, giving a voxel size of 0.94 × 0.94 × 1.2 mm^3, 140 sagittal slices, and the scanning time about 10 min. For each subject, both the MRI data sets were obtained in the same session.

Network construction

We constructed human brain WM networks based on the automated anatomical labeling (AAL) template (Tzourio-Mazoyer et al., 2002), which parcellates the human brain into 90 cortical and subcortical regions. The names and abbreviations of these brain regions are listed in Table 1. Each brain region was defined as a node and each detectable structural connection between a pair of nodes as an edge in a network. We analyzed the topological properties of the human brain WM networks using graph theory.

The procedure for constructing the brain WM networks is illustrated in Fig. 1 and can also be found in previous publications (Gong et al., 2009a; Lo et al., 2010; Wang et al., 2013a,b). First, we transformed the 90 brain regions from the Montreal Neurological Institute (MNI) space into individual diffusion space. For each subject, we coregistered the 3D brain structural images to the individual b_0 images (the less-distorted T2-weighted images acquired without diffusion weighting) using an affine registration. The resultant structural images in diffusion space were then mapped to the specific customized group T1 template in MNI space using a nonlinear transformation. An inverse transformation was used to warp the AAL template from MNI space to diffusion space by a nearest-neighbor interpolation method. The linear and nonlinear transformations were all performed using the SPM5 package (http://www.fil.ion.ucl.ac.uk/spm/software/spm5).

Next, we performed diffusion tensor tractography in each individual's diffusion space and obtained the WM fibers for the whole brain using DtiStudio (Jiang et al., 2006). Distortions due to the head motion and eddy current were corrected via an affine transformation in Anatomic Image Registration (AIR) within DtiStudio (Jiang et al., 2006). We then estimated the diffusion tensor and calculated the eigenvalues, eigenvectors, and the fractional anisotropy (FA) for each voxel. The WM fibers in the whole brain were reconstructed using the Fiber

Assignment by Continuous Tracking (FACT) algorithm, which was implemented in DtiStudio. Fiber tracking was terminated at voxels when FA < 0.25 and tracking turning angle > 45°. Afterward, we defined each edge of the human brain WM networks using the assumption that two brain regions were structurally connected if at least three streamlines ($n \geqq 3$) were detected between each pair of regions (Shu et al., 2011). Such a threshold selection may reduce the risk of false-positive connections due to noise or the limitations of the deterministic tractography. The weight of each edge, w_{ij}, was defined as FA × (FN $\geqq$ 3) (Lo et al., 2010), where FA refers to the mean FA value along the fiber bundles, FN to the value of the streamline counts, and FN $\geqq$ 3 to that the connection exists if at least three streamlines were detected between each pair of regions.

Network analysis

Global parameters. We utilized three parameters to measure the small-world property, specifically, the normalized weighted clustering coefficient, γ, normalized weighted characteristic path length, λ, and small-worldness, σ. A network can be considered to be small-world if $\gamma \gg 1$ and $\lambda \approx 1$ (Watts and Strogatz, 1998), and the small-worldness measure, σ, can be used to capture this property in a single quantitative parameter (Humphries et al., 2006). Furthermore, we used four other measures to characterize the global properties of brain WM networks: the weighted clustering coefficient, C_p, weighted characteristic path length, L_p, global efficiency, E_{glob}, and local efficiency, E_{loc}. Their definitions are provided in Table 2 and in Rubinov and Sporns (2010).

Regional parameters. We adopted the nodal efficiency, $E_{nodal}(i)$, degree, K_i, and betweenness centrality, B_i, to describe the nodal properties of the brain WM networks. Their definitions are also provided in Table 2 and in Rubinov and Sporns (2010).

Hubs refer to highly connected nodes in a network. In this study, we identified node i as a network hub if $E_{nodal}(i)$ satisfies the following criterion:

$$E_{nodal}(i) > mean + SD,$$

where *mean* and *SD* stand for the average nodal efficiency and the standard deviation of nodal efficiency over all nodes of the network, respectively.

Robustness analysis

Parcellation scheme. Zalesky et al. (2010) found that the network parameters vary considerably as a function of spatial scale: both σ and γ were increased but λ was kept stable when nodal spatial scale was made finer; both C_p and E_{glob} were decreased but L_p was increased when the number of nodes was raised up. These findings indicate that the spatial scale of the brain parcellation may affect the comparison of network parameters. In order to check the robustness of our network analysis, we adopted a higher-resolution human brain template, the AAL-1024 template, to re-calculate the topological properties of the networks for both the left mTLE patients and the controls. The calculation steps were exactly the same as the main scheme except for the respective change.

Edge schemes. Several previous studies (Shu et al., 2011; Zhang et al., 2014) evaluated the effect of different edge definitions on the network parameters and found no significant influence on the results. In this study, we further assigned different definitions of edge weight, FN, FA, and FA × (FN $\geqq n$), where n refers to the streamline counts ranging from one to five, to construct the brain WM networks. The aim was to test if different edge definitions affect the results.

Statistical analysis

A nonparametric permutation test (Bullmore et al., 1999) was performed to detect significant between-group difference in each of the global and nodal parameters between the left mTLE patients and the controls. Given a network parameter, we initially calculated the between-group difference of the mean values. For each permutation, we reallocated all subjects randomly into two groups and conducted two-sample two-tailed *t*-tests. This randomization procedure was repeated 10,000 times for the given network parameter and the corresponding distribution of t values was obtained. We set the critical values at 99% of the distribution for each of the global parameters and at 99.5% of the distribution for each of the nodal parameters for testing the null hypothesis. Before the permutation tests, we applied multiple linear regression analysis to remove the confounding factors of age and gender for each network parameter (Gong et al., 2009b). The false discovery rate (FDR) (Genovese et al., 2002) was used to control the multiple comparisons for each of the nodal parameters. Furthermore, we calculated the effect size and the statistical power according to Cohen (1992) and Suckling et al. (2010), respectively.

In addition, we performed a partial correlation analysis to detect the relationship between the network parameter and the duration as well as the onset age of disease in the left mTLE patients. Once a parameter with significant between-group difference was observed, we assessed the relationship between the parameter and the clinical data (duration and onset age of disease) by regressing out the confounding factors (age and gender).

RESULTS

Global properties

The normalized weighted clustering coefficient, γ, normalized weighted characteristic path length, λ, and small-worldness, σ, were calculated separately for the left mTLE patients and the controls. We found that for both groups, the values of γ were about three times larger than those of the random networks and the values of λ were approximately equivalent to those of the random networks (Fig. 2B). The values of ratio $\sigma = \gamma/\lambda$

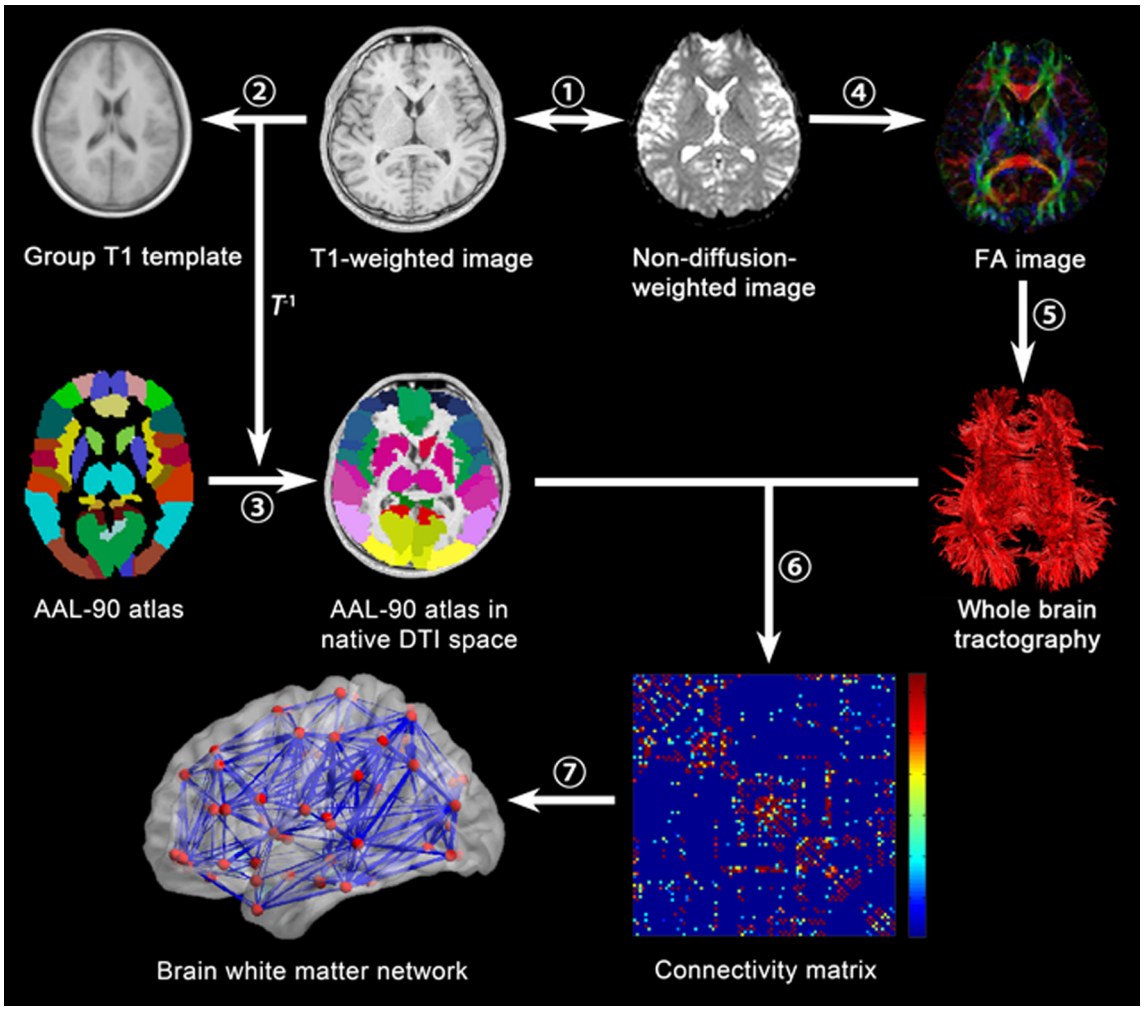

Fig. 1. Flowchart for the reconstruction of the human brain WM networks. (1) Rigid co-registration of the T1-weighted brain structural images to the native DTI space. (2) Nonlinear transformation of the co-registered T1-weighted images to the same stereotactic space as the customized template image. (3) The inverse transformation was applied to warp the automated anatomical labeling (AAL) template from the MNI space to the native DTI space. (4) Estimation of the diffusion tensor to obtain eigenvalues and eigenvectors for each voxel. (5) Reconstruction of the whole-brain white matter fibers using DtiStudio with FACT algorithm. (6) Construction of the weighted brain WM network for each subject. Edge weight was defined as the product of the streamline counts (*FN*) and the mean fractional anisotropy (*FA*) of the fiber bundles connecting each pair of brain regions. (7) Rendering plot of the weighted brain WM networks (plotted using BrainNet Viewer, Version 1.1, Beijing Normal University, http://www.nitrc.org).

were larger than 1 for both groups (Fig. 2B). These findings suggest that the brain WM networks for both the left mTLE patients and the controls held prominent small-world properties. Table 3 lists details of the small-world properties of brain networks for each group.

Fig. 2A shows statistical comparisons for the global parameters of the brain networks between the left mTLE patients and the controls. We found the weighted characteristic path length (L_p) was significantly increased, but the global efficiency (E_{glob}) was significantly decreased in the left mTLE patients compared to the controls (Fig. 2A). On the other side, we found no significant difference in the clustering coefficient (C_p) or the local efficiency (E_{loc}) between the two groups (Fig. 2A). Table 3 lists the details of between-group comparisons for the global parameters. The results indicate that the global properties were markedly altered in the brain WM networks of the left mTLE patients compared to the controls.

Nodal parameters

In the present study, we utilized the nodal efficiency (E_{nodal}), degree (K_i), and betweenness centrality (B_i) to characterize the nodal parameters of the 90 brain regions.

Table 4 lists the brain regions with significant differences in nodal properties between the left mTLE patients and the controls. Considering that none of them survived FDR correction, we applied a less stringent false positive correction $p < 0.005$ to determine the alteration of nodal parameters in the left mTLE patients. Seven brain regions were found to have significant between-group differences both in nodal efficiency and in degree, named the left superior temporal gyrus (STG.L), the right middle temporal gyrus (MTG.R), superior temporal pole (TPOsup.R), middle temporal pole (TPOmid.R), superior occipital gyrus (SOG.R), middle occipital gyrus (MOG.R), and middle frontal gyrus (MFG.R). We also observed significant between-group difference in nodal efficiency in the left hippocampus (HIP.L), and significant

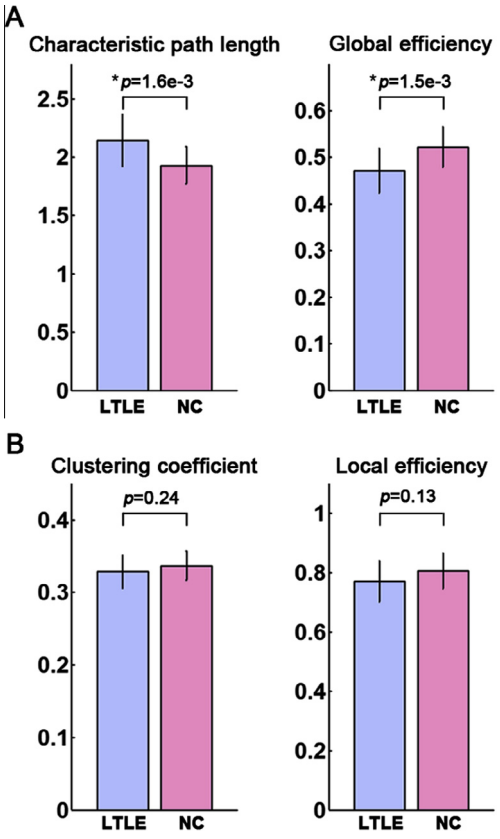

Fig. 2. Network metrics of the left mTLE patients and the normal controls (NC) changing with different definitions of edge weight FA $\times$ (FN $\geqq$ n), where n ranged from 1 to 5. (A) Global parameters: clustering coefficient, characteristic path length, global efficiency, and local efficiency. The global parameters with significant between-group differences are indicated by an asterisk above the corresponding FN threshold ($p < 0.01$). (B) Small-world properties: the normalized weighted clustering coefficient, γ, normalized weighted characteristic path length, λ, and small-worldness, σ.

between-group difference in degree in the right median cingulate and paracingulate gyri (DCG.R). These regions are also presented in Fig. 3.

Network hubs. We identified 18 hub regions for the left mTLE patients, including 13 association cortex regions, three primary cortex regions, and two paralimbic regions. While for the controls, we identified 16 hub regions, including 11 association cortex regions, three primary cortex regions, and two paralimbic regions. Among these hub regions, 16 hub regions were the same for both groups, including the bilateral medial superior frontal gyrus (SFGmed), bilateral supplementary motor area (SMA), left dorsolateral superior frontal gyrus (SFGdor.L), left middle frontal gyrus (MFG.L), left precentral gyrus (PreCG.L), left postcentral gyrus (PoCG.L), left superior parietal gyrus (SPG.L), left inferior parietal lobule (IPL.L), left middle occipital gyrus (MOG.L), right cuneus (CUN.R), right precuneus (PCUN.R), right calcarine fissure (CAL.R), right anterior cingulate and paracingulate gyri (ACG.R), and right median cingulate gyri (DCG.R). Two hub regions, the right lingual gyrus (LING.R) and the left precuneus (PCUN.L), were specific to the left mTLE patients. The hub regions are displayed in Fig. 4. We can see that even though the rankings of the hub regions were very similar for the two groups, the distribution of the hub regions was changed indeed. This may further indicate the alteration of the global metrics of the brain WM networks while the small-worldness kept in the left mTLE patients.

Correlations between network parameters and clinical data of the left mTLE patients

The correlation analysis detected no significant correlation between any of the global parameters and the duration or the onset age of the left mTLE patients. For the nodal properties, we found that the degree in MTG.R was significantly negatively correlated with the duration of the disease ($r = -0.64$, $p = 0.02$), the nodal efficiency of TPOmid.R and STG.L was marginally negatively associated with the duration ($r = -0.58$, $p = 0.0504$), and the onset age ($r = -0.57$, $p = 0.0551$) of the left mTLE patients, respectively.

Robustness analysis

In order to check the robustness of our results, we repeated the network analysis for both the left mTLE patients and the controls by adopting the following two procedures.

Parcellation scheme. We selected a high-resolution brain parcellation scheme, the AAL-1024 template, to define the nodes, and repeated the network analysis. We found that the brain WM networks for both groups still held small-world properties ($\gamma \gg 1$, $\lambda \approx 1$; and $\sigma > 1$) (Table 3), and detected significantly decreased E_{glob} but significantly increased L_p in the left mTLE patients compared to the controls. These results were similar to those derived from the AAL-90 template. However, we observed significantly decreased C_p and E_{loc} in the left mTLE patients compared to the controls, which were not found in the network analysis based on the AAL-90 template.

Edge scheme. We found that the two groups always kept the small-worldness in the definitions of edge weight FA $\times$ (FN $\geqq$ n) (the streamline counts n = 1, 2, 3, 4, 5) (Fig. 2B). When taking FA or FN as the edge weight, we found the brain WM networks of each group also held prominent small-world properties ($\gamma \gg 1$; $\lambda \approx 1$; $\sigma > 1$). For the networks constructed from these different definitions of edge weights, we found consistent significant differences in E_{glob} and L_p between the left mTLE patients and the controls, while C_p and E_{loc} were kept unchanged at the same time. These results were obviously in accordance with our main results as we selected FA $\times$ (FN $\geqq$ 3) as the edge weight. The detailed information of the network parameters corresponding to different definitions of edge weight is listed in Tables 5 and 6.

DISCUSSION

Using diffusion tensor tractography and graph theory, we compared the topological properties of brain WM

Table 3. Global parameters and small-world properties of the networks derived from the AAL-90 and AAL-1024 templates between the left mTLE patients and the controls

Network parameters	AAL-90					AAL-1024				
	mTLE patients	Normal Controls	*p* value	Effect size (*d*)	Power	mTLE patients	Normal Controls	*p* value	Effect size (*d*)	Power
C_p	0.33 ± 0.02	0.34 ± 0.02	0.24	–	–	0.22 ± 0.02	0.25 ± 0.02	3.00e−4	1.02	0.83
L_p	2.15 ± 0.22	1.93 ± 0.16	1.60e−3	1.17	0.92	6.45 ± 1.00	5.14 ± 0.73	1.00e−4	1.54	0.99
E_{glob}	0.47 ± 0.05	0.52 ± 0.04	1.50e−3	1.13	0.90	0.16 ± 0.03	0.20 ± 0.03	2.00e−4	1.39	0.98
E_{loc}	0.77 ± 0.07	0.81 ± 0.06	0.13	–	–	0.44 ± 0.06	0.51 ± 0.06	9.00e−4	1.03	0.84
γ	4.39 ± 0.35	4.01 ± 0.42	–	–	–	32.31 ± 4.15	33.56 ± 4.81	–	–	–
λ	1.13 ± 0.04	1.14 ± 0.04	–	–	–	1.45 ± 0.09	1.37 ± 0.07	–	–	–
σ	3.89 ± 0.26	3.53 ± 0.37	–	–	–	22.39 ± 3.43	24.48 ± 2.97	–	–	–

Abbreviations: C_p, clustering coefficient; L_p, characteristic path length; E_{glob}, global efficiency; E_{loc}, local efficiency; γ, normalized clustering coefficient; λ, normalized shortest path length; σ, small-worldness.

networks between left mTLE patients and the controls on a system level. The main findings are as follows: (i) the brain WM networks of the left mTLE patients were significantly different from those of the controls, as indicated by a significant increase in characteristic path length but a significant decrease in global efficiency; and (ii) the nodal parameters were significantly decreased in the STG.L, hippocampus, and the right occipital and temporal cortices in the left mTLE patients compared to the controls. This implies a disruption of large-scale brain WM networks in the left mTLE patients, which is in accord with previous studies based on other imaging methods (Liao et al., 2010; Bernhardt et al., 2011).

In this study, the brain WM networks for both the left mTLE patients and the controls exhibited prominent small-world properties. This finding was kept consistent under a high-resolution brain parcellation scheme (Table 3) and different definitions of edge weight (Fig. 2). This result is in line with a recent DTI-based network analysis by Liu et al. (2014) and also previous network studies based on other imaging techniques (for reviews, see (Bullmore and Sporns, 2009; He and Evans, 2010)).

We also found significantly increased L_p but significantly decreased E_{glob} in the left mTLE patients compared to the controls. From Table 3 and Fig. 2, we found these results were relatively consistent in the brain WM networks constructed with different definitions of node and edge weight. As described by Watts and Strogatz (1998), L_p is defined as the average number of edges in the shortest paths between all nodal pairs to reflect the integration or information transfer capacity between and across remote cortical regions, while E_{glob} is a topological measure of reciprocal or inverse of the path length between nodes to indicate the overall capacity for parallel information transfer and integrated processing in brain networks (Latora and Marchiori, 2001; Bullmore and Sporns, 2012). These two measures are inversely proportional to each other. L_p is primarily influenced by long paths (infinitely long paths), while E_{glob} is primarily influenced by short paths (Rubinov and Sporns, 2010). Therefore, the alterations of L_p and E_{glob} may reflect disruption of the global integration of the brain WM networks or impaired structural connections in the left mTLE patients. On the other hand, the unchanged values of C_p and E_{loc}, both of which are related to short-range connections between neighboring regions (Watts and Strogatz, 1998; Latora and Marchiori, 2001), may suggest retention of local segregation of the brain WM networks in the left mTLE patients. Our results were in line with several previous DTI studies, which directly showed disrupted structural integrity in some specific WM tracts, such as the corpus callosum (Meng et al., 2010), fornix, cingulum (Concha et al., 2009), uncinate fasciculus, arcuate fasciculus (Lin et al., 2008), and inferior fronto-occipital fasciculus (McDonald et al., 2008a). Our findings are consistent with a recent DTI study by Liu et al. (2014)

Table 4. Brain regions with significant differences in nodal properties between the left mTLE patients and the controls ($p < 0.005$, uncorrected). For the abbreviations of the nodes, see Table 1

Brain regions	Nodal efficiency			Degree		
	p value	Effect size (*d*)	Power	*p* value	Effect size (*d*)	Power
MOG.R	5.00e−4	1.43	0.98	4.00e−4	1.48	0.99
SOG.R	5.00e−4	1.24	0.94	1.80e−3	1.02	0.83
MFG.R	2.30e−3	1.18	0.92	4.30e−3	1.11	0.89
TPOmid.R	2.40e−3	0.87	0.69	2.80e−3	1.00	0.81
MTG.R	3.30e−3	1.07	0.86	2.50e−3	0.97	0.79
STG.L	3.80e−3	1.07	0.86	3.70e−3	1.08	0.87
HIP.L	4.00e−3	1.09	0.88	–	–	–
TPOsup.R	4.30e−3	1.00	0.82	4.60e−3	0.97	0.79
DCG.R	–	–	–	5.00e−3	0.99	0.80

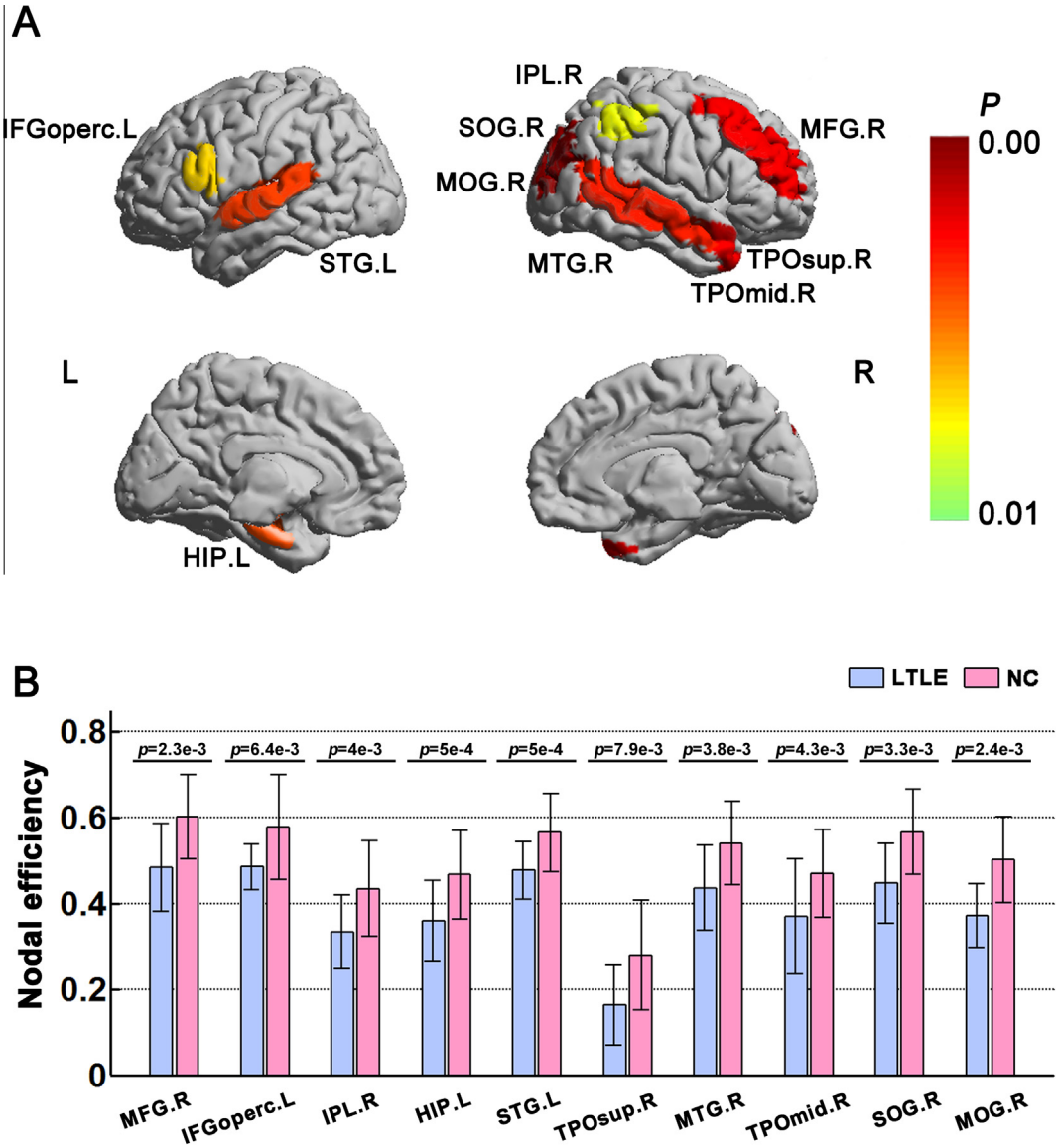

Fig. 3. Surface-rendered view and bar plot of brain regions with significant differences in the nodal parameters between the left mTLE patients and the normal controls (NC) ($p < 0.005$, uncorrected). (A) Nodal efficiency. (B) Degree. The bar height and the half error bar represent the mean value and the standard deviation of the nodal properties in the corresponding region for each group, respectively. All of the nodal properties for the left mTLE patients were decreased compared to those of the controls. Differences in nodal parameters between the left mTLE and NC were shown in the range of $0 < p < 0.005$, colored from red to blue. For abbreviations of the nodes, see Table 1. (For interpretation of the references to colour in this figure legend, the reader is referred to the web version of this article.)

detecting concurrent decreases of global and local efficiencies. However, we noticed that our finding of the unchanged path length was not in line with that reported in the study. In another study based on cortical thickness correlations, Bernhardt et al. (2011) found an increased path length, which is consistent with our study; while on the other hand demonstrated increased clustering in TLE although we found no difference in it between patients and controls. Using resting-state fMRI, Liao et al. (2010) reported a decreased clustering coefficient and shorter path length in TLE with bilateral MTS. And Wang et al. (2014) detected significant increases in clustering coefficient and characteristic path length, but a decrease in global efficiency in the TLE patients compared to the controls. The different sample size, recruit criteria, modalities, definitions of the nodes and edges used in network construction may contribute to the discrepancy between these findings.

In addition, we found widespread brain regions showed alterations of nodal properties between the left mTLE patients and the controls. Give a node, the nodal efficiency measures its connectivity to all the other nodes in the network, and quantifies the importance of the node for the communication within the network (Achard and Bullmore, 2007; Gong et al., 2009b). Thus, alterations in the nodal efficiency reflect abnormalities in inter-regional connectivity. We observed reduced nodal efficiency in the HIP.L (Fig. 3A), which is consistent with

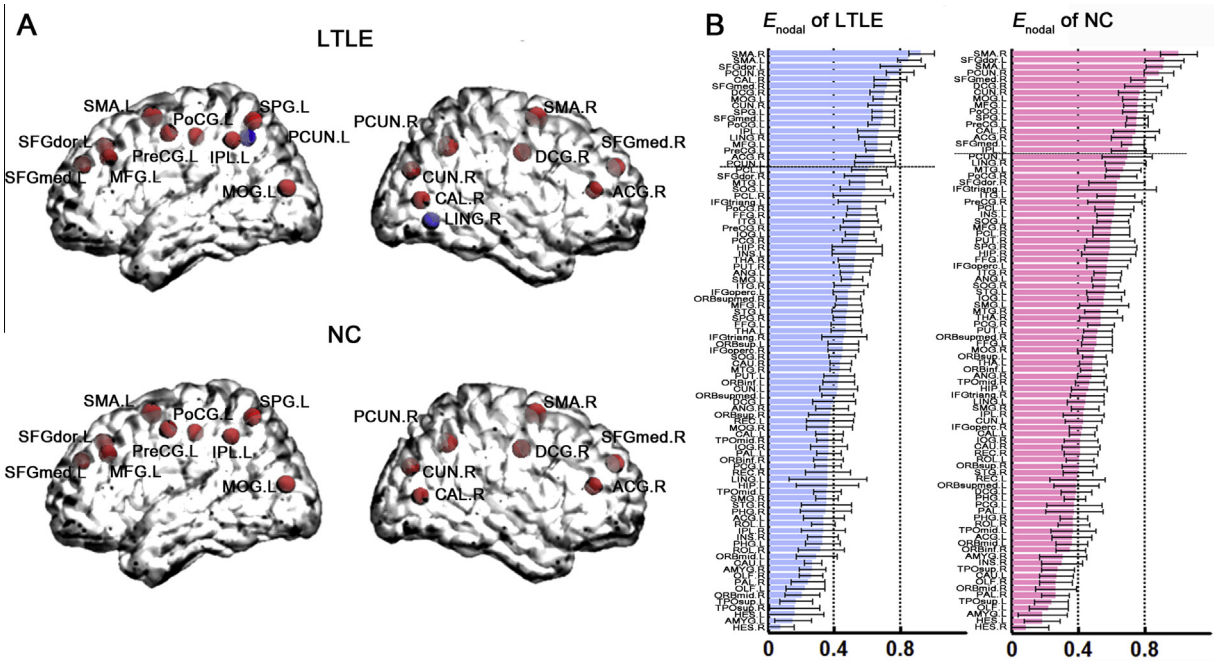

Fig. 4. Hub regions of the human brain white matter networks for both the left mTLE patients and the normal controls (NC). Hubs were identified based on the criterion of $E_{nodal}(i) > mean + SD$ for each of the subject groups. $E_{nodal}(i)$ means the nodal efficiency of node *i*. (A) Hub distributions for both groups. Nodes color-coded in red were shared by both groups. Nodes color-coded in blue were specific to the left mTLE patients. (B) The 90 brain regions were sorted in descending order for each group. The dashed line indicates the threshold of determining a hub in each group. Abbreviations of the nodes can be found in Table 1. (For interpretation of the references to colour in this figure legend, the reader is referred to the web version of this article.)

a recent DTI study showing a significantly reduced nodal efficiency in the ipsilateral hippocampus in the limbic network in left mTLE patients (Bonilha et al., 2012). Previous studies (Focke et al., 2008; Keller et al., 2009; Li et al., 2012) also reported alterations in diffusion indices, FA and mean diffusivity (MD), in the ipsilateral hippocampus in the left mTLE patients. Meanwhile, we found the left mTLE patients showed significantly reduced nodal properties in STG.L (Fig. 3), which is believed to be involved in the understanding of written and spoken language (Turkeltaub et al., 2002; Seger et al., 2013). Several DTI studies (Lin et al., 2008; Kim et al., 2011; Scanlon et al., 2013) reported that abnormal FA and apparent diffusion coefficient (ADC) in left mTLE patients were located in the ipsilateral uncinate fasciculus and arcuate fasciculus, which connect STG and the other regions. And several morphological studies (McDonald et al., 2008b; Riederer et al., 2008) also found decreased gray matter volume in STG in left mTLE patients. From Fig. 3, we found most of regions with altered nodal properties in the left mTLE patients were located in the right occipital and temporal cortices (Fig. 3). The finding of impairment of the occipital cortex in the left mTLE is consistent with previous studies. With the voxel-based analysis, Shon et al. (2010) found significantly increased MD in the contralateral occipital regions in left mTLE patients, and Lin et al. (2007) detected significantly decreased cortical thickness in the occipital regions in the left mTLE. Using the independent component analysis (ICA), Voets et al. (2009) revealed significant reductions in functional

Table 5. Statistical comparisons of the global parameters of brain structural networks between the left TLE patients with mesial temporal sclerosis (mTLE) and the healthy controls derived from different definitions of edge weight (FA, FN, and FA × FN). FA, the mean fractional anisotropy of the fiber bundles connecting a pair of brain regions; FN, the streamline counts between a pair of brain regions. FN ⩾ *n* refers to the structural connection exists if at least n streamlines were detected between a pair of regions

Definition of edge weight	C_p			L_p			E_{glob}			E_{loc}		
	p value	Effect size (*d*)	Power	*p* value	Effect size (*d*)	Power	*p* value	Effect size (*d*)	Power	*p* value	Effect size (*d*)	Power
FA	0.63	–	–	4.00e−4	1.32	0.97	1.20e−3	1.30	0.96	0.40	–	–
FN	0.28	–	–	1.70e−3	1.15	0.91	2.00e−3	1.13	0.90	0.12	–	–
FA × (*FN*⩾1)	0.17	–	–	2.30e−3	1.10	0.88	3.70e−3	1.07	0.86	0.03	–	–
FA × (*FN*⩾2)	0.48	–	–	2.10e−3	1.10	0.88	3.90e−3	1.06	0.86	0.10	–	–
FA × (*FN*⩾4)	0.10	–	–	6.00e−4	1.22	0.94	1.50e−3	1.17	0.92	0.07	–	–
FA × (*FN*⩾5)	0.05	–	–	5.00e−4	1.28	0.96	8.00e−4	1.23	0.94	0.04	–	–

Table 6. Statistical comparisons of nodal properties of the brain structural networks for the left TLE patients with mesial temporal sclerosis (mTLE) and the controls derived from various definitions of edge weight (*FA*, *FN*, and *FA* × *FN*). All the nodal parameters in the left mTLE patients were significantly decreased compared to the controls. The between-group differences in the nodal parameters were computed with age and gender as confounding covariates. *FA*, the mean fractional anisotropy of the fiber bundles connecting a pair of brain regions; *FN*, the streamline counts between a pair of brain regions. $FN \geqslant n$ refers to the structural connection exists if at least *n* streamlines were detected between a pair of regions. Abbreviations of brain regions are listed in Table 1

Edge weight definition: FA								Edge weight definition: FN							
Nodal efficiency				Degree				Nodal efficiency				Degree			
Brain regions	*p* value	Effect size (*d*)	Power	Brain regions	*p* value	Effect size (*d*)	Power	Brain regions	*p* value	Effect size (*d*)	Power	Brain regions	*p* value	Effect size (*d*)	Power
OLF.L	4.00e−04	1.25	0.95	TPOsup.R	2.00e−04	1.33	0.97	MOG.R	3.00e−04	1.41	0.98	MOG.R	4.00e−04	1.44	0.99
OLF.R	1.10e−03	1.29	0.96	OLF.L	1.40e−03	1.14	0.90	SOG.R	1.50e−03	1.16	0.92	TPOmid.R	1.80e−03	1.03	0.84
SFGmed.R	9.00e−04	1.01	0.82	INS.L	2.10e−03	1.22	0.94	MFG.R	1.60e−03	1.20	0.93	SOG.R	1.90e−03	1.03	0.84
INS.L	1.20e−03	1.31	0.96	SFGmed.R	3.90e−03	0.79	0.61	TPOmid.R	1.80e−03	0.85	0.68	STG.L	2.30e−03	1.11	0.89
ACG.R	4.10e−03	0.95	0.78	IPL.R	4.10e−03	1.10	0.88	STG.L	2.80e−03	1.15	0.91	MFG.R	2.40e−03	1.15	0.91
SOG.R	3.60e−03	1.12	0.89	TPOmid.R	4.50e−03	1.09	0.88	TPOsup.R	2.80e−03	1.03	0.84	MTG.R	3.10e−03	0.96	0.79
IOG.R	9.00e−04	1.19	0.92					MTG.R	3.90e−03	1.04	0.85	SPG.R	3.40e−03	0.98	0.80
IPL.R	2.70e−03	1.11	0.88					IFGoperc.L	4.00e−03	0.96	0.78	TPOsup.R	4.50e−03	0.99	0.81
TPOsup.R	1.10e−03	1.17	0.92					PUT.L	4.90e−03	0.80	0.63				
TPOmid.R	2.80e−03	1.1	0.88					HIP.L	4.90e−03	1.05	0.85				
Edge weight definition: FA × (FN ≧ 1)								Edge weight definition: FA × (FN ≧ 2)							
Nodal efficiency				Degree				Nodal efficiency				Degree			
Brain regions	*p* value	Effect size (*d*)	Power	Brain regions	*p* value	Effect size (*d*)	Power	Brain regions	*p* value	Effect size (*d*)	Power	Brain regions	*p* value	Effect size (*d*)	Power
MOG.R	4.00e−04	1.42	0.98	MOG.R	5.00e−04	1.49	0.99	MOG.R	3.00e−04	1.38	0.98	MOG.R	3.00e−04	1.47	0.99
SOG.R	1.10e−03	1.20	0.93	TPOmid.R	2.60e−03	0.97	0.79	SOG.R	1.10e−03	1.19	0.93	TPOmid.R	2.70e−03	0.98	0.79
MFG.R	3.90e−03	1.10	0.88	SOG.R	3.10e−03	1.02	0.83	MFG.R	3.30e−03	1.11	0.89	MTG.R	2.80e−03	0.95	0.77
MTG.R	4.10e−03	1.06	0.86	TPOsup.R	4.00e−03	0.99	0.81	TPOmid.R	3.40e−03	0.85	0.68	SOG.R	3.60e−03	1.00	0.82
				MTG.R	4.50e−03	0.97	0.79	MTG.R	4.20e−03	1.04	0.84	STG.L	4.80e−03	1.05	0.85
								TPOsup.R	4.40e−03	0.98	0.80	DCG.R	4.80e−03	0.98	0.79
								STG.L	4.80e−03	1.01	0.83				
Edge weight definition: FA × (FN ≧ 4)								Edge weight definition: FA × (FN ≧ 5)							
Nodal efficiency				Degree				Nodal efficiency				Degree			
Brain regions	*p* value	Effect size (*d*)	Power	Brain regions	*p* value	Effect size (*d*)	Power	Brain regions	*p* value	Effect size (*d*)	Power	Brain regions	*p* value	Effect size (*d*)	Power
MOG.R	1.00e−04	1.46	0.99	MOG.R	6.00e−04	1.48	0.99	MOG.R	3.00e−04	1.48	0.99	MOG.R	5.00e−04	1.48	0.99
SOG.R	1.40e−03	1.29	0.96	SOG.R	2.00e−03	1.04	0.84	SOG.R	4.00e−04	1.48	0.99	SOG.R	1.30e−03	1.05	0.85
MFG.R	1.90e−03	1.19	0.93	TPOmid.R	2.70e−03	0.97	0.79	MFG.R	1.30e−03	1.25	0.95	DCG.R	2.40e−03	1.04	0.84
TPOsup.R	3.10e−03	1.02	0.83	MTG.R	3.20e−03	0.98	0.79	MTG.R	1.80e−03	1.10	0.88	MFG.R	2.80e−03	1.14	0.90
MTG.R	3.10e−03	1.08	0.87	STG.L	4.70e−03	1.04	0.85	TPOmid.R	2.10e−03	0.88	0.71	MTG.R	2.80e−03	0.98	0.80
STG.L	3.40e−03	1.07	0.86	DCG.R	4.80e−03	1.00	0.81	HIP.L	2.50e−03	1.13	0.90	TPOmid.R	2.90e−03	0.98	0.80
TPOmid.R	3.50e−03	0.86	0.69	TPOsup.R	5.00e−03	0.98	0.79	TPOsup.R	2.50e−03	1.04	0.84	STG.L	4.00e−03	1.07	0.86
HIP.L	4.60e−03	1.10	0.88					STG.L	3.80e−03	1.11	0.89	IPL.R	4.80e−03	1.05	0.85
								IFGoperc.L	4.80e−03	0.96	0.78				

connectivity between bilateral middle temporal cortices, bilateral occipital and left orbitofrontal regions in left mTLE group. Our results showed both ipsilateral and contralateral abnormalities in nodal properties of the left mTLE group, which are consistent with those of Liu et al. (2014), in which patients with mTLE were found to show widespread reduction of regional efficiency in ipsilateral temporal, bilateral frontal, and bilateral parietal areas. Taken together, we may suggest that the brain WM network in patients with left mTLE is disrupted, and mTLE is a systemic brain disorder. In brief, our findings are consistent with the extensive brain structural abnormalities in the left mTLE patients.

For correlations between the topological parameters and the clinical evaluation, we observed the degree in MTG.R was significantly negatively correlated with the duration of the disease. The degree of an individual node is equal to the number of edges connected to that node, which reflects importance of nodes in the network. Previous functional neuroimaging studies (Tranel et al., 1997; Chao et al., 1999; Cabeza and Nyberg, 2000) have suggested that the middle temporal gyrus is involved in language and semantic memory processing. The negative correlation between the degree in MTG and the disease duration may indicate the adverse effect of the disease on the condition of the brain region.

Limitations

First, the DTI data with non-isotropic voxel size and low signal-to-noise ratio (SNR) (acquired from a 1.5T MRI scanner) may bias the calculation result. To address the potential effects of non-isotropic voxel size and low SNR, we repeated the network analysis using different inter-regional connectivity threshold and different brain parcellation schemes, and found that the results showed a high robustness across subjects. This suggests that our findings are reliable, although some suboptimal scanning parameters were used here. Using similar DTI parameters, several recent studies also reported a high reproducibility of the WM network properties (Gong et al., 2009a; Shu et al., 2011). No doubt, we should acquire DTI datasets with optimal sequence parameters for further analysis (Posnansky et al., 2011).

Second, the selection of FA threshold may influence the result of network analysis. TLE patients show reduced FA in many tracts according to previous studies (Concha et al., 2009; Meng et al., 2010). In this study, we adopted the threshold of FA > 0.25 for fiber tracking. Previously, we found that the choices of the FA thresholds have significant effects on the topological parameters of the brain WM networks (Wang et al., 2013a,b). As the FA increased, the characteristic path length increases, while clustering coefficient, global efficiency and local efficiency decreased. Thus, the effect of the selection of FA threshold on the network analysis in TLE patients may be worth further investigation.

Finally, we only enrolled a small sample of the left mTLE patients in a cross-sectional design to show alterations in the topological properties of the brain WM networks. That may be the reason why none of the nodal properties survived FDR correction. A longitudinal and larger-sample study would be vital to demonstrate progressive alterations in the brain WM networks in TLE.

In summary, we investigated the brain WM organizations in TLE patients from a system level by using diffusion tensor tractography and graph theory. Statistical analyses showed that the global properties of brain WM networks were significantly altered in the left mTLE patients compared to the controls. We also found that nodal properties were significantly changed in the widespread brain regions in the left mTLE patients which corroborates the impairment of the extensive brain regions. The correlation analysis showed the negative relationship between the clinical data and the nodal properties, indicating a negative effect of the disease on the brain WM networks in the left mTLE patients. Our findings may help to understand the clinical symptoms of TLE patients and may offer a clue for the diagnosis and treatment to the TLE patients in the future.

CONFLICT OF INTEREST

The authors declare that the research was conducted is the absence of any commercial or financial relationships that should be construed as a potential conflict of interest.

Acknowledgments—This work was partly supported by the Nanfang Hospital of the Southern Medical University and the Guangdong 999 Brain Hospital, the funding of the National Natural Science Foundation of China (Grant numbers: 81071149, 81271548, 81271389, and 81371535), the Science and Technology Planning Project of Guangdong Province (2011b060200002), and the Scientific Research Foundation for Returned Overseas Chinese Scholars (RH), State Education Ministry. The authors express appreciation to Drs. Rhoda E. and Edmund F. Perozzi for editing assistance. The authors thank the two anonymous reviewers for their constructive comments and their suggestions.

REFERENCES

Achard S, Bullmore E (2007) Efficiency and cost of economical brain functional networks. PLoS Comput Biol 3:174–183.

Alessio A, Pereira FRS, Sercheli MS, Rondina JM, Ozelo HB, Bilevicius E, Pedro T, Covolan RJM, Damasceno BP, Cendes F (2013) Brain plasticity for verbal and visual memories in patients with mesial temporal lobe epilepsy and hippocampal sclerosis: an fMRI study. Human Brain Mapp 34:186–199.

Bai F, Shu N, Yuan Y, Shi Y, Yu H, Wu D, Wang J, Xia M, He Y, Zhang Z (2012) Topologically convergent and divergent structural connectivity patterns between patients with remitted geriatric depression and amnestic mild cognitive impairment. J Neurosci 32:4307–4318.

Bernhardt BC, Bernasconi N, Concha L, Bernasconi A (2010) Cortical thickness analysis in temporal lobe epilepsy reproducibility and relation to outcome. Neurology 74:1776–1784.

Bernhardt BC, Chen Z, He Y, Evans AC, Bernasconi N (2011) Graph-theoretical analysis reveals disrupted small-world organization of cortical thickness correlation networks in temporal lobe epilepsy. Cereb Cortex 21:2147–2157.

Bernhardt BC, Rozen DA, Worsley KJ, Evans AC, Bernasconi N, Bernasconi A (2009) Thalamo-cortical network pathology in idiopathic generalized epilepsy: insights from MRI-based morphometric correlation analysis. NeuroImage 46:373–381.

Bernhardt BC, Worsley KJ, Besson P, Concha L, Lerch JP, Evans AC, Bernasconi N (2008) Mapping limbic network organization in temporal lobe epilepsy using morphometric correlations: Insights on the relation between mesiotemporal connectivity and cortical atrophy. NeuroImage 42:515–524.

Bonilha L, Nesland T, Martz GU, Joseph JE, Spampinato MV, Edwards JC, Tabesh A (2012) Medial temporal lobe epilepsy is associated with neuronal fibre loss and paradoxical increase in structural connectivity of limbic structures. J Neurol Neurosurg Psychiatr 83:903–909.

Bullmore E, Sporns O (2009) Complex brain networks: graph theoretical analysis of structural and functional systems. Nat Rev Neurosci 10:186–198.

Bullmore E, Sporns O (2012) The economy of brain network organization. Nat Rev Neurosci 13:336–349.

Bullmore ET, Suckling J, Overmeyer S, Rabe-Hesketh S, Taylor E, Brammer MJ (1999) Global, voxel, and cluster tests, by theory and permutation, for a difference between two groups of structural MR images of the brain. IEEE Trans Med Imaging 18:32–42.

Cabeza R, Nyberg L (2000) Imaging cognition II: An empirical review of 275 PET and fMRI studies. J Cognit Neurosci 12:1–47.

Chao LL, Haxby JV, Martin A (1999) Attribute-based neural substrates in temporal cortex for perceiving and knowing about objects. Nat Neurosci 2:913–919.

Cohen J (1992) A power primer. Psychol. Bull. 112:155.

Concha L, Beaulieu C, Collins DL, Gross DW (2009) White-matter diffusion abnormalities in temporal-lobe epilepsy with and without mesial temporal sclerosis. J Neurol Neurosurg Psychiatr 80:312–319.

Engel J (2001) Mesial temporal lobe epilepsy: what have we learned? Neuroscientist 7:340–352.

Focke NK, Yogarajah M, Bonelli SB, Bartlett PA, Symms MR, Duncan JS (2008) Voxel-based diffusion tensor imaging in patients with mesial temporal lobe epilepsy and hippocampal sclerosis. NeuroImage 40:728–737.

Genovese CR, Lazar NA, Nichols T (2002) Thresholding of statistical maps in functional neuroimaging using the false discovery rate. NeuroImage 15:870–878.

Gong G, He Y, Concha L, Lebel C, Gross DW, Evans AC, Beaulieu C (2009a) Mapping anatomical connectivity patterns of human cerebral cortex using in vivo diffusion tensor imaging tractography. Cereb Cortex 19:524–536.

Gong G, Rosa-Neto P, Carbonell F, Chen ZJ, He Y, Evans AC (2009b) Age- and gender-related differences in the cortical anatomical network. J Neurosci 29:15684–15693.

Guye M, Bettus G, Bartolomei F, Cozzone PJ (2010) Graph theoretical analysis of structural and functional connectivity MRI in normal and pathological brain networks. MAGMA 23:409–421.

Hagmann P, Cammoun L, Gigandet X, Meuli R, Honey CJ, Wedeen VJ, Sporns O (2008) Mapping the structural core of human cerebral cortex. PLoS Biol 6:1479–1493.

He Y, Evans A (2010) Graph theoretical modeling of brain connectivity. Curr Opin Neurol 23:341–350.

Humphries MD, Gurney K, Prescott TJ (2006) The brainstem reticular formation is a small-world, not scale-free, network. Proc Biol Sci 273:503–511.

Iturria-Medina Y, Sotero RC, Canales-Rodriguez EJ, Aleman-Gomez Y, Melie-Garcia L (2008) Studying the human brain anatomical network via diffusion-weighted MRI and Graph Theory. NeuroImage 40:1064–1076.

Jiang HY, van Zijl PCM, Kim J, Pearlson GD, Mori S (2006) DtiStudio: resource program for diffusion tensor computation and fiber bundle tracking. Comput Methods Programs Biomed 81:106–116.

Keller SS, Baker G, Downes JJ, Roberts N (2009) Quantitative MRI of the prefrontal cortex and executive function in patients with temporal lobe epilepsy. Epilepsy Behav 15:186–195.

Keller SS, Roberts N (2008) Voxel-based morphometry of temporal lobe epilepsy: an introduction and review of the literature. Epilepsia 49:741–757.

Kim CH, Chung CK, Koo BB, Lee JM, Kim JS, Lee SK (2011) Changes in language pathways in patients with temporal lobe epilepsy: diffusion tensor imaging analysis of the uncinate and arcuate fasciculi. World Neurosurg 75:509–516.

Latora V, Marchiori M (2001) Efficient behavior of small-world networks. Phys Rev Lett 87:198701.

Li J, Zhang Z, Shang H (2012) A meta-analysis of voxel-based morphometry studies on unilateral refractory temporal lobe epilepsy. Epilepsy Res 98:97–103.

Liao W, Zhang Z, Pan Z, Mantini D, Ding J, Duan X, Luo C, Lu G, Chen H (2010) Altered functional connectivity and small-world in mesial temporal lobe epilepsy. PLoS One 5:e8525.

Lin JJ, Riley JD, Juranek J, Cramer SC (2008) Vulnerability of the frontal–temporal connections in temporal lobe epilepsy. Epilepsy Res 82:162–170.

Lin JJ, Salamon N, Lee AD, Dutton RA, Geaga JA, Hayashi KM, Luders E, Toga AW, Engel Jr J, Thompson PM (2007) Reduced neocortical thickness and complexity mapped in mesial temporal lobe epilepsy with hippocampal sclerosis. Cereb Cortex 17:2007–2018.

Liu M, Chen Z, Beaulieu C, Gross DW (2014) Disrupted anatomic white matter network in left mesial temporal lobe epilepsy. Epilepsia 55:674–682.

Lo C-Y, Wang P-N, Chou K-H, Wang J, He Y, Lin C-P (2010) Diffusion tensor tractography reveals abnormal topological organization in structural cortical networks in Alzheimer's disease. J Neurosci 30:16876–16885.

McDonald CR, Ahmadi ME, Hagler DJ, Tecoma ES, Iragui VJ, Gharapetian L, Dale AM, Halgren E (2008a) Diffusion tensor imaging correlates of memory and language impairments in temporal lobe epilepsy. Neurology 71:1869–1876.

McDonald CR, Hagler Jr DJ, Ahmadi ME, Tecoma E, Iragui V, Gharapetian L, Dale AM, Halgren E (2008b) Regional neocortical thinning in mesial temporal lobe epilepsy. Epilepsia 49:794–803.

Meng L, Xiang J, Kotecha R, Rose D, Zhao H, Zhao D, Yang J, Degrauw T (2010) White matter abnormalities in children and adolescents with temporal lobe epilepsy. Magn Reson Imaging 28:1290–1298.

Posnansky O, Kupriyanova Y, Shah NJ (2011) On the problem of gradient calibration in diffusion weighted imaging. Int J Imaging Syst Technol 21:271–279.

Riederer F, Lanzenberger R, Kaya M, Prayer D, Serles W, Baumgartner C (2008) Network atrophy in temporal lobe epilepsy – a voxel-based morphometry study. Neurology 71:419–425.

Rubinov M, Sporns O (2010) Complex network measures of brain connectivity: uses and interpretations. NeuroImage 52:1059–1069.

Salvador R, Suckling J, Coleman MR, Pickard JD, Menon D, Bullmore E (2005) Neurophysiological architecture of functional magnetic resonance images of human brain. Cereb Cortex 15:1332–1342.

Scanlon C, Mueller SG, Cheong I, Hartig M, Weiner MW, Laxer KD (2013) Grey and white matter abnormalities in temporal lobe epilepsy with and without mesial temporal sclerosis. J Neurol 260:2320–2329.

Seger CA, Spiering BJ, Sares AG, Quraini SI, Alpeter C, David J, Thaut MH (2013) Corticostriatal contributions to musical expectancy perception. J Cognit Neurosci 25:1062–1077.

Shon YM, Kim YI, Koo BB, Lee JM, Kim HJ, Kim WJ, Ahn KJ, Yang DW (2010) Group-specific regional white matter abnormality revealed in diffusion tensor imaging of medial temporal lobe epilepsy without hippocampal sclerosis. Epilepsia 51:529–535.

Shu N, Liu Y, Li K, Duan Y, Wang J, Yu C, Dong H, Ye J, He Y (2011) Diffusion tensor tractography reveals disrupted topological efficiency in white matter structural networks in multiple sclerosis. Cereb Cortex 21:2565–2577.

Suckling J, Barnes A, Job D, Brenan D, Lymer K, Dazzan P, Marques TR, MacKay C, McKie S, Williams SR (2010) Power calculations for multicenter imaging studies controlled by the false discovery rate. Human Brain Mapp 31:1183–1195.

Tranel D, Damasio H, Damasio AR (1997) A neural basis for the retrieval of conceptual knowledge. Neuropsychologia 35:1319–1327.

Turkeltaub PE, Eden GF, Jones KM, Zeffiro TA (2002) Meta-analysis of the functional neuroanatomy of single-word reading: Method and validation. NeuroImage 16:765–780.

Tzourio-Mazoyer N, Landeau B, Papathanassiou D, Crivello F, Etard O, Delcroix N, Mazoyer B, Joliot M (2002) Automated anatomical labeling of activations in SPM using a macroscopic anatomical parcellation of the MNI MRI single-subject brain. NeuroImage 15:273–289.

Vaessen MJ, Jansen JFA, Vlooswijk MCG, Hofman PAM, Majoie HJM, Aldenkamp AP, Backes WH (2012) White matter network abnormalities are associated with cognitive decline in chronic epilepsy. Cerebral Cortex 22:2139–2147.

Voets NL, Adcock JE, Stacey R, Hart Y, Carpenter K, Matthews PM, Beckmann CF (2009) Functional and structural changes in the memory network associated with left temporal lobe epilepsy. Hum Brain Mapp 30:4070–4081.

Waites AB, Briellmann RS, Saling MM, Abbott DF, Jackson GD (2006) Functional connectivity networks are disrupted in left temporal lobe epilepsy. Ann Neurol 59:335–343.

Wang B, Fan Y, Lu M, Li S, Song Z, Peng X, Zhang R, Lin Q, He Y, Wang J, Huang R (2013a) Brain anatomical networks in world class gymnasts: a DTI tractography study. NeuroImage 65:476–487.

Wang J, Qiu S, Xu Y, Liu Z, Wen X, Hu X, Zhang R, Li M, Wang W, Huang R (2014) Graph theoretical analysis reveals disrupted topological properties of whole brain functional networks in temporal lobe epilepsy. Clin Neurophysiol.

Wang SL, Jingtai Liu, Ruibin Zhang, Yong Xu, Gaolang Gong, Yong He, Ruiwang Huang (2013) Effects of tractographic parameters on the topological measures of the brain anatomical networks. The 19th Annual Meeting of the Organization for Human Brain Mapping 5404.

Watts DJ, Strogatz SH (1998) Collective dynamics of 'small-world' networks. Nature 393:440–442.

Zalesky A, Fornito A, Harding IH, Cocchi L, Yuecel M, Pantelis C, Bullmore ET (2010) Whole-brain anatomical networks: Does the choice of nodes matter? NeuroImage 50:970–983.

Zalesky A, Fornito A, Seal ML, Cocchi L, Westin C-F, Bullmore ET, Egan GF, Pantelis C (2011) Disrupted Axonal Fiber Connectivity in Schizophrenia. Biol Psychiatry 69:80–89.

Zhang R, Wei Q, Kang Z, Zalesky A, Li M, Xu Y, Li L, Wang J, Zheng L, Wang B, Zhao J, Zhang J, Huang R (2014) Disrupted brain anatomical connectivity in medication-naïve patients with first-episode schizophrenia. Brain Struct Funct:1–15.

(Accepted 25 August 2014)
(Available online 3 September 2014)